International Journal of Solids and Structures 139–140 (2018) 129–137

Contents lists available at ScienceDirect

International Journal of Solids and Structures

journal homepage: www.elsevier.com/locate/ijsolstr

Influence of prior cyclic plasticity on creep deformation using crystal plasticity modelling

T.O. Erinosho*, K. Abburi Venkata, M. Mostafavi, D.M. Knowles, C.E. Truman

Solid Mechanics Group, Department of Mechanical Engineering, University of Bristol, Bristol BS8 1TR, UK

ARTICLE INFO

Article history:
Received 25 September 2017
Revised 14 January 2018
Available online 31 January 2018

Keywords:
Crystal plasticity
Creep
Fatigue
Prior plasticity
Finite element analysis

ABSTRACT

This paper proposes a simple, yet effective, modified crystal plasticity framework which is capable of modelling plasticity and creep deformation. In particular, the proposed model is sufficiently versatile to capture the effects of complex load histories on polycrystals, representative of those experienced by real materials in industrial plant. Specifically, the methodology was motivated by the need in the power generation industry to determine whether cyclic pre-straining influences the subsequent creep behaviour of type 316H austenitic stainless steel as compared to non-cyclically pre-strained material. Cyclic pre-straining occurs widely in plant and it is of paramount importance to accurately account for its impact on the subsequent deformation and integrity of relevant components.

The framework proposed in this paper considers the effects of dislocation glide and climb in a relatively simple manner. It is calibrated using experimental tests on 316H stainless steel subjected solely to monotonic plasticity and forward creep. Predictions are then obtained for the creep response of the same material after it had been subjected to cycles of pre-strain. The predictions are compared to experimental results and good agreement was observed. The results show slower creep strain accumulation following prior cyclic loading attributed to hardening structures developed in the material during the cyclic pre-strain. The model also highlights the importance of accounting for directionality of hardening under reverse loading. This is hypothesized to affect the development of an internal stress state at an intragranular level which is likely to affect subsequent creep accumulation.

1. Introduction

This paper proposes a plasticity and creep deformation model within a crystal plasticity finite element framework and uses it to investigate the influence of cyclic pre-strain on creep in type 316H stainless steel. The behaviour of stainless steel in various creep regimes has been extensively reported in the literature due to its wide range of applications in the power generation industry (Mehmanparast et al., 2016; Mehmanparast et al., 2013; Hong et al., 2016). Creep in metals is defined as time-dependent permanent deformation which occurs under an applied stress typically when the temperature (T) exceed $0.5T_m$, where T_m is the melting temperature of the metal (Edward and Ashby, 1979). In dislocation creep, the high temperature and stress provide the energy required for immobilized dislocations to climb to a coplanar slip plane, thus overcoming the obstacles due to dislocation traps such as jogs/kinks or precipitates. The resulting climb assisted glide leads to time-dependent permanent deformations known as creep deformation (Weertman, 1955).

Studies have shown that the dislocation creep response of a component is influenced by its prior plastic loading history (Mehmanparast et al., 2016; Mikami, 2016; Marnier et al., 2016; Joseph et al., 2013; Esztergar, 1972; Wei and Dyson, 1982). However, the significance of the influence of monotonic/cyclic pre-straining remains uncertain and has been debated (Joseph et al., 2013). Wei and Dyson (1982) observed that higher plastic pre-straining of 316 stainless steel, up to 1.5% tensile strain, increases its subsequent creep life. Hong et al. (2016) experiments on 347 stainless steel showed that monotonically pre-straining samples up to 30% plastic strain at 650 °C and then applying stresses greater than 200 MPa increases its creep life compared to lower levels of pre-straining. They attributed this behaviour to the formation of twinning due to the high pre-existing deformation which acts as a barrier to dislocation glide. Conversely, low levels of pre-strain accelerate strain-induced precipitation of sigma phases at grain boundaries that act at sites of creep cav-

* Corresponding author.
E-mail address: tomiwa.erinosho@bristol.ac.uk (T.O. Erinosho).

https://doi.org/10.1016/j.ijsolstr.2018.01.028

Nomenclature

All quantities are dimensionless unless otherwise stated

$\boldsymbol{F}$	total deformation gradient
$\boldsymbol{F^p}$	plastic deformation gradient
$\boldsymbol{F^e}$	elastic deformation gradient
$\boldsymbol{I}$	identity Matrix
$\boldsymbol{\gamma^\alpha}$	slip on slip system $\boldsymbol{\alpha}$ ($\mathbf{s}^{-1}$)
$\boldsymbol{n^\alpha}$	slip plane $\boldsymbol{\alpha}$
$\boldsymbol{s^\alpha}$	slip direction $\boldsymbol{\alpha}$
$\boldsymbol{L^p}$	plastic velocity gradient
$\boldsymbol{\Omega^p}$	spin
$\boldsymbol{\dot{\gamma}^\alpha}$	alip rate on slip system $\boldsymbol{\alpha}$
$\boldsymbol{D^p}$	symmetric part of velocity gradient
$\boldsymbol{\Omega^e}$	asymmetric part of velocity gradient
$\boldsymbol{\dot{\gamma}_0}$	reference slip rate ($\mathbf{s}^{-1}$)
$\boldsymbol{\tau^\alpha}$	shear stress on slip system $\boldsymbol{\alpha}$
$\boldsymbol{h_0}$	hardening modulus (Pa)
$\boldsymbol{g^\alpha}$	slip strength on slip system $\boldsymbol{\alpha}$
$\mathfrak{H}$	dislocation climb softening factor
$\boldsymbol{\gamma_{sum}}$	accumulated slip
$\boldsymbol{\sigma_{vm}}$	Von Mises stress (Pa)
$\boldsymbol{\psi}$	activation energy (J)
$\boldsymbol{k}$	Boltzmann constant ($\mathbf{m^2kgs^{-2}K^{-1}}$)
$\boldsymbol{T}$	temperature (K)
$\boldsymbol{T_m}$	melting temperature (K)
$\boldsymbol{\Delta\varepsilon}$	strain range
$\boldsymbol{N_{slip}}$	number of slip systems
$\boldsymbol{\tau_0}$	critical resolved shear stress (Pa)
$\boldsymbol{\varepsilon_{max}}$	maximum applied strain
$\boldsymbol{\varepsilon_{min}}$	minimum applied strain

ity formation and therefore reduce the tertiary stage of creep life. Murakami et al. (1990) reported that the creep life of type 316 stainless steel is reduced when it is subjected to cyclic pre-straining. Joseph et al. (2013) observed a factor between two and six for the increase in creep life (at 550 °C) of samples which had experienced pre-straining. Mikami's (2016) conclusion that cyclic pre-straining reduces creep life at 650 °C were reconfirmed by Skelton RP (1999) and Takahashi (2015).

The review above reveals that there is considerable uncertainty in evaluating the influence of prior plastic strain on the creep deformation of materials. Experimental complexities associated with the details of loading or unloading during the transition to creep are rarely reported in the literature and could have a profound effect on the measured results. For example, pre-straining in tension or compression, or at high or room temperature prior to creep is likely to influence the nature of creep strain accumulation. Considering the long-term duration of creep experiments, carrying out a comprehensive systematic experimental study to investigate the effects of key parameters on the creep deformation of critical components in the energy industry would be prohibitively costly and time consuming. Details associated with the transition between plasticity and creep in experiments, as well as the wide range of non-proportional strain paths that may be explored, makes a systematic experimental study unfeasible. There is therefore a paramount need to develop a mechanistic model which can correctly simulate the effects of various initial conditions, such as non-proportional straining, on the creep deformation of materials.

Attempts have been made to develop continuum and microstructure-based creep models (Agarwal et al., 2007; Dunne and Hayhurst, 2016; Manonukul et al., 2002; Dunne et al., 1990; Venkatramani et al., 2007; Li et al., 2014; Golden et al., 2014). Studies such as Agarwal et al. (2007), Bower and Wininger (2004) and Dyson (2000) have developed detailed continuum creep deformation and damage models implemented into finite element methods to evaluate the constitutive response of polycrystals during high temperature loading. However, traditional continuum approaches are limited in their ability to account for the influence of local variations at the intragranular scale, such as the distribution of internal stress which is crucial to processes such as creep (Chen et al., 2014). Internal stress here is generally defined as the grain level intergranular orientation dependent stresses developed within the polycrystal model (Roters et al., 2010). Within the grains a distinct internal (intragranular) stress may evolve as a function of the underlying deformation constitutive relations. During creep, stress redistribution will depend on the local crystallographic orientation of that particular grain as well as the incompatibility between neighbouring grains (Pommier et al., 2016). The incompatibility component is typically accounted for in continuum approaches such as self-consistent models (SCM) using a backstress implemented into the constitutive equation, thereby accounting for long range stresses (Hu et al., 2016). This approach provides insights into the influence of kinematic effects on the yield surface evolution.

Given the inability to capture intragranular details in SCM, the crystal plasticity creep framework developed in this paper pursues a discretized finite element approach. This has the advantage of accounting for material microstructure and texture as well as capturing the locally acting mechanisms that drive deformation glide and climb of dislocations. Two approaches may be followed:

(a) Incorporate equations governing the dislocation climb motion into a framework which already describes the dislocation glide, i.e. plasticity. This approach is usually adopted within frameworks that directly simulate the dislocation motion such as discrete dislocation dynamics (Keralavarma et al., 2012; Danas and Deshpande, 2013). Such simulation techniques, although mechanistic, are often limited to modelling simple geometries. However, attempts have been made to implement climb assisted glide motions into higher length-scale modelling frameworks such as crystal plasticity (Geers et al., 2014). Such models require detailed analysis of the microstructure evolution and are often dependent on model calibrations using in-situ or ex-situ microstructural characterization of small scale creep tests.

(b) Rather than directly incorporating the dislocation climb equations in the simulation formulation, it is possible to model climb assisted glide by introducing softening terms within the framework. This approach accommodates relaxation processes which also consider mechanistic aspects of overcoming dislocation traps. It can readily be adopted in a crystal plasticity framework that is capable of simulating thousands of grains in components with complex geometries. Examples of this approach are described in Li et al. (2014) and Hu and Cocks (2016).

The aim of this paper is to develop a modelling framework that captures the effects of prior cyclic plastic strain on the primary and secondary stages of creep deformation. To achieve this, the previous experimental results which will be used to calibrate and validate our model are presented in Section 2 followed by a description of the creep-enabled crystal plasticity (CP) framework in Section 3. The framework is calibrated in Section 4 and in Section 5 the framework is used to determine the influence of prior cyclic plasticity on creep deformation. Discussions on the performance of the current model are presented in Section 6 and finally conclusions are drawn in Section 7.

2. Experimental data

The experimental results utilised in this paper have been previously reported in Joseph et al. (2013), thus will only be briefly reviewed here. Experiments were conducted at 823 K on specimens fabricated from type 316H stainless steel which had been extracted from an ex-service header supplied by EDF Energy. The cylindrical specimens had a diameter of 5.66 mm. The three key experiments that were used to inform the computational study reported in this paper are summarized below.

First, the time-independent mechanical response was obtained by subjecting the specimen to a displacement-controlled uniaxial test. The specimen was designed according to ASTM E8 (ASTM International 2016). The displacement-control test was carried out at 0.2 mm/min on a hydraulic test frame and the displacements were measured using a clip gauge. The mechanical response obtained was used to calibrate the time-independent crystal plasticity (CP) properties in the CP framework.

Second, time-dependent creep tests were carried out by applying uniaxial constant loads of 250 MPa and 300 MPa at 550 °C. It is worth highlighting that the time-independent inelastic strain accumulated whilst applying the initial load prior to hold was measured as 1.92% and 4.6% for loads of 250 MPa and 300 MPa, respectively. The specimens were then maintained at the respective loads and the total inelastic strain, which included the time-independent component in addition to the time-dependent component accumulated during hold, was measured using a LVDT.

Third, the influence of cyclic pre-strain on creep was evaluated by subjecting specimens to 37 fully reversed cycles ($R = \frac{\sigma_{min}}{\sigma_{max}} = -1$) under strain-control with a strain range ($\Delta\varepsilon$) of 0.8%. 37 pre-strain cycles were undertaken in order to attain peak hardening (N^{peak}) in the hysteresis loop. Following the cyclic loading, the samples were unloaded and then subjected to forward creep at 250 MPa as above. The plasticity developed by applying the initial 250 MPa was measured as 0.18%, which was much lower compared to the plastic strain accumulated at 250 MPa without cyclic pre-strain (1.92%). Next, the load was maintained at 250 MPa and the total inelastic strain comprising the initial time-independent plasticity (0.18%) plus the time-dependent inelastic strain was measured.

3. Creep-enabled crystal plasticity (CP) framework

3.1. Crystal plasticity finite element framework

The CP framework is derived in Lee (1969) in which the kinematic decomposition of the deformation gradient, $\boldsymbol{F}$, into elastic, $\boldsymbol{F}^*$, and plastic, $\boldsymbol{F}^{\text{p}}$, tensors is given by

$$\boldsymbol{F} = \boldsymbol{F}^*\boldsymbol{F}^p. \tag{1}$$

The deformation resulting from crystallographic slip, $\boldsymbol{F}^p$, is such that

$$\boldsymbol{F}^p = \boldsymbol{I} + \sum \gamma^\alpha (\boldsymbol{s}^\alpha \otimes \boldsymbol{n}^\alpha), \tag{2}$$

where $\boldsymbol{I}$ is the unity vector, $\boldsymbol{s}$ is the slip systems direction vector, $\boldsymbol{n}$ is the normal to those directions and, γ is slip on a given slip system α. The plastic part of the velocity gradient may be written as

$$\boldsymbol{L}^p = \sum \gamma^\alpha (\boldsymbol{s}^\alpha \otimes \boldsymbol{n}^\alpha) = \boldsymbol{D}^p + \boldsymbol{\Omega}^p, \tag{3}$$

where $\boldsymbol{D}^p$ and $\boldsymbol{\Omega}^p$ are the symmetric and antisymmetric parts of the plastic velocity gradient, respectively. The evolution of the crystallographic orientation is determined from the antisymmetric part of the elastic velocity gradient, $\boldsymbol{\Omega}^e$, given by

$$\boldsymbol{\Omega}^e = asym(\boldsymbol{L}) - \boldsymbol{\Omega}^p, \tag{4}$$

where crystallographic orientations are updated using $\boldsymbol{s}^{\alpha^*} = \boldsymbol{\Omega}^{\text{e}}\boldsymbol{s}^\alpha$ and $\boldsymbol{n}^{\alpha^*} = \boldsymbol{n}^\alpha\boldsymbol{\Omega}^{\text{e}-1}$ respectively. Note that $\boldsymbol{L} \approx \boldsymbol{L}^p$ assuming large deformation.

Numerous constitutive slip rules to describe the deformation on each slip system have been suggested by researchers (Li et al., 2014; Golden et al., 2014; Erinosho et al., 2013b; Sun et al., 2016; Forest and Rubin, 2016; Cheong et al., 2007). We have employed a power law relationship between slip rate and resolved shear stress to describe the full range of dislocation controlled plasticity such that

$$\dot{\gamma}^\alpha = \dot{\gamma}_0 \left| \frac{\tau^\alpha}{g^\alpha} \right|^n sgn(\dot{\gamma}). \tag{5}$$

In Eq. (5), the slip rate along the αth slip system, $\dot{\gamma}^\alpha$, evolves on individual slip systems and depends on the reference strain rate, $\dot{\gamma}_0$, resolved shear stress in that slip system, τ^α, and slip system resistance, g^α. A hardening law based on a McGinty and McDowell (2004) formulation is employed here which defines the slip system resistance by

$$\dot{g}^\alpha = \text{ɾ}h_0\left(1 + \frac{h_0\gamma_{\text{sum}}}{\tau_0 m}\right)^{m-1}\dot{\gamma}^\alpha, \tag{6}$$

where $\dot{g}^\alpha$, the rate of slip system resistance, is an indicator of the resistance to dislocation motion, and $\gamma_{\text{sum}} = \sum_{\alpha=1}^{N_{\text{slip}}} \int |\dot{\gamma}^\alpha| dt$ represents the accumulated plasticity on all slip systems, N_{slip}. γ_{sum} provides an interaction between slip systems such that slip on a particular slip system α in addition to slip on other systems both contribute to the level of hardening attained on that system (i.e. self and latent hardening are not distinguished). The hardening modulus h_0, and fitting parameter, m, are determined for a particular material; note that m determines the rate of saturation of accumulated strain. τ_0 is a constant dquantifying the value of the critical resolved shear stress, g_0, where g_0 is the initial slip resistance and thus representative of the undeformed state of the material. A multiplication term, ɾ, has been added to the original McGinty and McDowell (2004) hardening law. ɾ, a dislocation climb softening factor, is a modifier used here to account for the time-dependent response of dislocation motion and is discussed in detail in the next section. The formulation presented above has been implemented for the twelve slip systems, $\{111\}<1\bar{1}0>$, present in Face Centred Cubic (FCC) crystals. These have been incorporated into an ABAQUS user material subroutine details of which have been discussed elsewhere (Kysar, 1997).

3.2. Creep methodology

A forward creep experiment comprises a uniaxial loading, denoted as phase 1, followed by a hold at constant load, denoted as phase 2. This is shown schematically in Fig. 1(a). Phase 1, which has a very short time-period, can be considered as the accumulation of time-independent plasticity whereas the accumulated inelastic strain during phase 2 is time-dependent i.e. climb-assisted dislocation glide. The dislocation-induced creep strain response follows the profile shown in Fig. 1(b) and comprises a primary, secondary and tertiary stages of creep. Our focus is on the creep deformation in the primary and secondary stages.

The primary stage of creep shown schematically in Fig. 1(b) usually has a very short duration and involves the pinning of dislocations at obstacles. This is captured using the conventional hardening term on each slip system, g^α, in the CP framework by specifying ɾ = 1 during this phase. The hardening accumulated saturates, causing the strain rate to decrease to its minimum value. The secondary creep stage is captured by evolving the dislocation climb softening factor, ɾ, in the hardening law. ɾ reduces the level of hardening at high temperatures. The total inelastic strain refers to

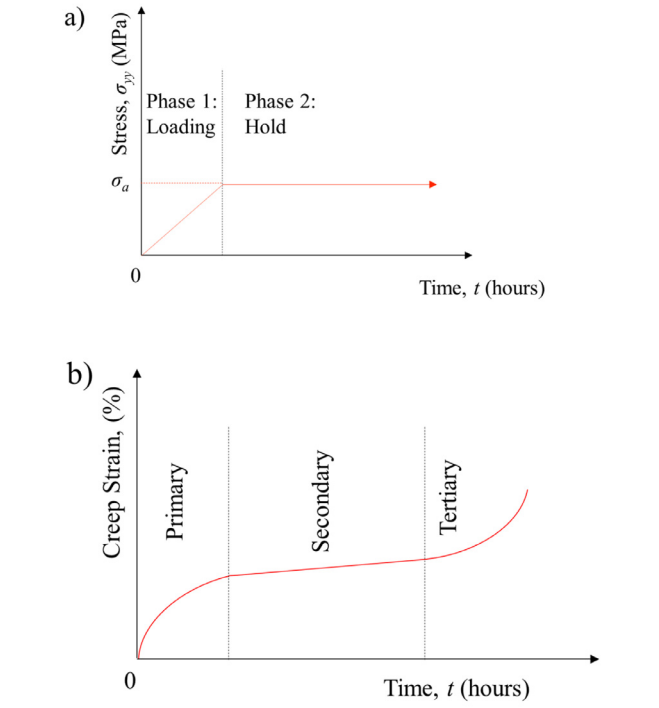

Fig. 1. Schematic showing (a) loading sequence in a forward creep test (b) the evolution of creep strain with time (c) sequence cyclic preloading followed by of a forward creep test.

the summation of time-independent strain which is derived from conventional crystal plasticity based on dislocation glide plus the time-dependent inelastic strain developed due to creep, i.e. climb assisted dislocation glide.

The term $\mathfrak{Y}$ is calculated from a temperature and local stress dependent hardening factor ϕ through

$$\mathfrak{Y} = \frac{1}{\phi}, \tag{7}$$

where

$$\phi = A \cdot \left(e^{-\frac{\psi}{kT}}\right) \cdot \sigma_{\mathrm{vm}}^{p} + 1. \tag{8}$$

ψ is the activation energy in Joules, k is the Boltzmann constant in $\mathrm{m^2\,kg\,s^{-2}\,K^{-1}}$, T is the temperature in Kelvin and σ_{vm}

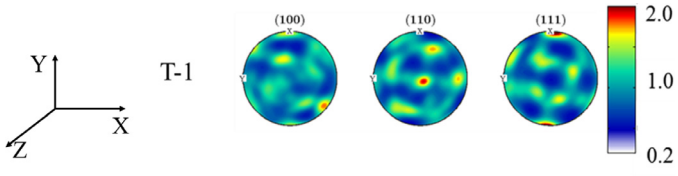

Fig. 2. The initial, relatively random, texture of the austenitic steel used in the analyses.

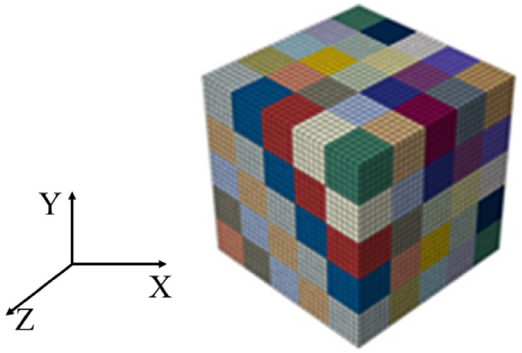

Fig. 3. Polycrystal model with 512 grains. Each grain ($25 \times 25 \times 25\mu\mathbf{m}^3$) is denoted as a region of similar colour and meshed using $6 \times 6 \times 6$ elements. Cubic grains are adopted because grain morphology effects are ignored.

is the local von Mises equivalent stress in Pa while A, a fitting factor that is expressed in $\mathrm{Pa^{-1}}$. The dimensionless parameter $\mathfrak{Y}$ is justified through a consideration of the underpinning physical laws. The dislocation climb softening behaviour is a diffusion process with a negligible effect over the short periods representative of time-independent plasticity, during which $\mathfrak{Y} = 1$. However, during creep deformation, $\mathfrak{Y}$ evolves which leads to a further accumulation of inelastic strain after time independent plasticity. During creep, the dislocation climb softening factor models the climb of vacancies in the lattice structure. This time dependent process is simulated through $\mathfrak{Y}$ since the local stress, σ_{vm}, is calculated iteratively. The resulting evolution of $\mathfrak{Y}$ as a function of stress (σ_{vm}) is shown in Fig. 5. In the time-independent phase $\mathfrak{Y}$= 1 and does not evolve with stress i.e. its evolution is switched off. However, the evolution of $\mathfrak{Y}$ is switched on at each integration point in the polycrystal during creep. Other components of the creep formulation presented here include temperature, T, and activation energy, ψ, which indicates the energy required to climb an obstacle.

The methodology presented here unifies the inelastic strain derived from time-independent and time-dependent inelasticity. This is unique because it provides the ability to account for the influence of plasticity on creep.

4. CP model and material properties

4.1. Initial texture and finite element model

An initial texture representative of the ex-service 316H stainless steel used in this research is illustrated as an orientation distribution map in Fig. 2. This texture was incorporated into the CP model shown in Fig. 3. Each separate colour in Fig. 3 defines a grain and all cubic elements (of type C3D8R) within this region are specified with the same orientation. Each grain comprises 216 elements following previous sensitivity studies on the appropriate model size and mesh density level (Erinosho and Dunne, 2014). Cubic grains of dimension $(25 \times 25 \times 25) \times 10^{-6}\mathrm{m}^3$ were adopted because previous work showed that the deformation was largely uninfluenced by grain morphology (Golden et al., 2014). Furthermore, whilst it is also possible to consider other textures, this texture was con-

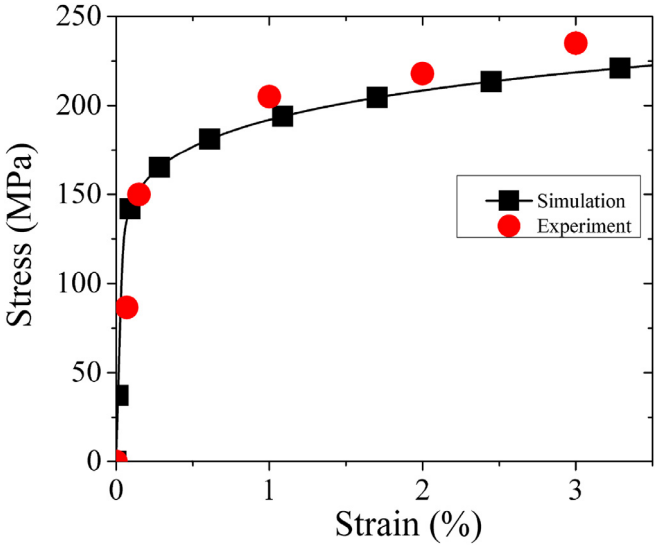

Fig. 4. Calibration of the crystal plasticity finite element parameters using experimental data for austenitic steel subjected to uniaxial straining 8. Note, 1-in-50 and 1-in-10 data points are shown for the experiment and crystal plasticity simulations respectively.

sidered for simplicity in order to demonstrate the applicability of the proposed framework. It is worth pointing out that the texture shown has a small preference in the *Y*-direction of the (111) planes, evident by the red hotspot in the pole figures. The (110) planes have a preference for the *Z*-direction.

Planar boundary conditions were applied to all surfaces of the polycrystal which was modelled assuming quarter symmetry. Planar boundary conditions were adopted because deformation was expected to be driven by the bulk response of the polycrystal. Therefore the influence of surface effects was expected to be very small (Erinosho and Dunne, 2014).

4.2. Calibration of time-independent plasticity properties

The initial plasticity material properties were calibrated by subjecting the +Y surface of the polycrystal shown in Fig. 2 to displacement-controlled uniaxial straining and equating the calculated mechanical response, i.e. the stress-strain curve, with that measured experimentally, as shown in Fig. 4. Based on the experimental stress-strain response a mean value of $g_0 = \tau_0 = 60 \times 10^6$Pa was adopted as the initial slip resistance for the twelve FCC slip systems. The hardening modulus $h_0 = 5 \times 10^9$Pa, and a fitting parameter $m = 0.245$, were representative constants obtained from the literature for FCC steels (McGinty and McDowell, 2004). For simplicity, the initial slip rate $\dot{\gamma}_0$ was set at unity and the strain rate sensitivity n in Eq. (5) was specifically minimized by choosing an appropriate value. A value of $n = 40$ was selected as it had been justified in earlier studies by the author (Erinosho et al., 2013a). Other properties included an Elastic modulus $E = 210 \times 10^9$Pa and a Poisson's ratio $\upsilon = 0.3$ (Chen et al., 2014). A bulk elastic modulus was utilised due to the largely random nature of the texture, thus limiting any anisotropy effects. The dislocation climb softening factor, $\mathfrak{s}$, was set to one when calibrating the time-independent plasticity properties as described in the previous section.

4.3. Calibration of time-dependent plasticity properties

Once determined, the time-independent parameters determined in Section 4.3 were considered fixed. The time-dependent (creep) parameters were calibrated using the forward creep tests described in Section 2. Accordingly, the activation energy $\psi = 4 \times 10^{-19}$J (Bower and Wininger, 2004; Webster and Ainsworth, 1994), temperature $T = 823$ K and $A = 1$ Pa^{-1}. Boltzmann's constant, k, is given by 1.38×10^{-23}m^{2}kg s^{-2}K^{-1} (Webster and Ainsworth, 1994). Finally, by fixing all the aforementioned parameters, $p = 1.75$ in Eq. (8) was calibrated such that the calculated rate of creep strain accumulated at differing applied stress levels agreed with the values obtained experimentally at 250×10^6Pa, 260×10^6Pa, 280×10^6Pa and 300×10^6Pa during primary and secondary creep. The experimental results are compared with those obtained using the calibrated crystal plasticity simulations in Fig. 6. A good agreement in creep response is observed for the two stress levels shown in Fig. 6 in the primary and secondary stages of creep.

5. Influence of cyclic pre-strain on creep

It was observed that 6 cycles of $\Delta\varepsilon = 0.8\%$ zero mean stress were required to attain peak hardening in the CP model. This differed from the experiment in which 37 cycles of pre-strain were needed to attain peak hardening. This is illustrated in Fig. 7. This difference was attributed to the fact that the initial time-independent CP properties were calibrated using uniaxial data. Hence, a uniaxial hardening response was used to predict the cyclic plasticity behaviour, which resulted in an overestimation of the accumulated hardening. Nevertheless, the accumulated hardening in experiment and simulation can be directly compared as both reach hysteresis saturation. The impact of this approach will be discussed in Section 6.3.

Upon subjecting the model to subsequent forward creep at 250 MPa following cyclic pre-strain to equivalent hardening levels, the inelastic strain response could be determined. The initial plastic strain calculated in CP following cyclic pre-strain and the application of the 250 MPa load was 0.17% compared to 0.18% measured experimentally. Subsequently, the creep rate accumulation was captured as shown in Fig. 8. It can be seen there is a good agreement between experiment and simulation. It is seen in Fig. 8 that cyclic pre-strain leads to a lower rate of accumulation of creep strain compared to that generated without pre-strain. This is attributed to the development formation of hardening structures discussed later in Section 6.

The CP polycrystal was further scrutinised by examining non-peak hardening cases. Six cases of cyclic pre-strain (0, 2, 3, 6, 7 and 8 cycles) were considered. For each case, the number of cycles specified was applied such that the final unloading was from both a tensile state and a compressive state. For example, applying one cycle starting in tension leads to the final unloading from a compressive state and vice versa. In both these cases, the model was subsequently subjected to forward creep at 250 MPa. For example, one pre-strain cycle refers to loading from zero to peak displacement in tension followed by reverse loading in compression and then unloading. Following this, forward creep at 250 MPa was applied. The objective was to evaluate the evolution of the internal stress state developed in the CP model. In effect, the orientation dependent stresses developed in the CP model (internal stresses) following applied cyclic loading with final unloading in tension and compression and its subsequent effect on forward creep was evaluated.

The results of the simulation detailed in the previous paragraph are shown in Table 1. Specifically, the difference in the magnitude of the creep strain accumulated after 1500 hours for a typical hold stress of 250 MPa after initial unloading from both tensile and compressive states was determined. A representative internal stress value was then determined by finding the difference in forward creep stress level required to achieve the same level of creep strain, assuming no cyclic pre-strain. The results show negligible internal stresses for all of the cases considered. This may be anticipated at peak hardening (6 or more cycles for the pa-

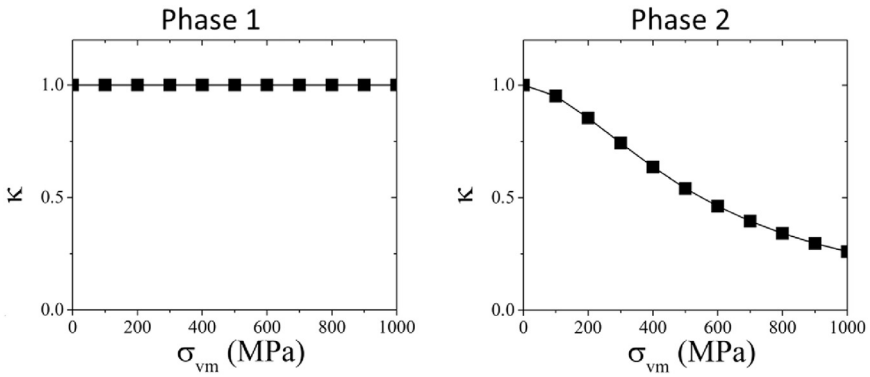

Fig. 5. Evolution of the dislocation climb softening parameter, κ, with effective stress, σ_{vm}, during phases 1 and 2 (see Fig. 1 for the definition of phases).

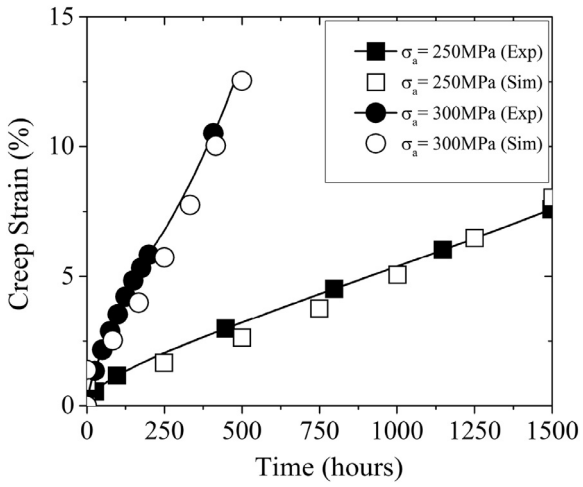

Fig. 6. Comparison between experimental creep strain and that calculated using the CP framework; 1-in-400 points are shown for the experimental results.

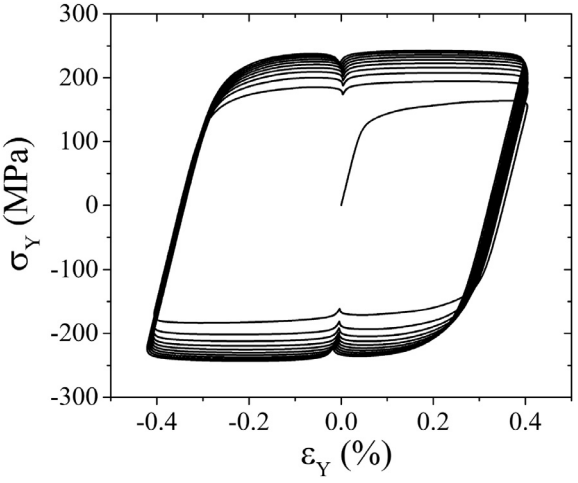

Fig. 7. Mechanical response of the CP polycrystal shown in Fig. 3 subjected to 10 cycles of $\Delta\varepsilon = 0.8\%$, $R = -1$, uniaxial loading.

Table 1
Estimates of the magnitude of internal stress state generated as a result of cyclic pre-straining (with final unloading in tension and compression) followed by forward creep. The results shown assumed an applied stress of 250 MPa with a 1500 h hold time.

Number of pre-strain cycles					
0	2	3	6	7	8
0 MPa	0.05 MPa	0.06 MPa	0.06 MPa	0.06 MPa	0.06 MPa

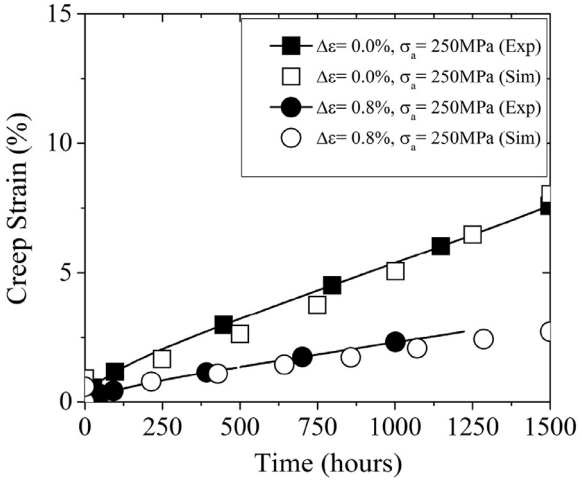

Fig. 8. The influence of prior cyclic plasticity on creep strain. The results with no cyclic pre-strain, $\Delta\varepsilon = 0\%$, are compared with those obtained with cyclic pre-straining. Following the pre-strain, forward creep was applied at an applied stress of 250 MPa.

rameters used here) but a more significant internal stress was expected prior to peak hardening (5 or fewer cycles.) The behaviour predicted was attributed to the inability of the underlying current model to account for the directionality of hardening, which has not been captured fully by the effect of a random microstructure simulated here. This is further discussed in the next section.

6. Discussion

6.1. Discretised CP model framework

The creep-enabled crystal plasticity model presented in this paper has been developed by incorporating a dislocation climb softening factor in the otherwise time-independent crystal plasticity finite element framework developed previously by the authors (Erinosho et al., 2013b). Of particular interest is the variety of constitutive relationships, such as the hardening behaviour and slip laws, proposed in the literature. For example, Dunne et al. (2007) developed a physically-based hyperbolic hardening function which was used to investigate cold dwell in Titanium polycrystals. Other studies have adopted various power law relationships (Erinosho et al., 2013b; Sun et al., 2016; Forest and Rubin, 2016). One commonality of all previous studies is the evolution of deformation, which has been constrained by a slip resistance described in this work (see Eq. (6)). However, the major difference between previous studies has been in the evolution of slip

resistance. Li et al. (2014) and Golden et al. (2014) adopted a slip resistance whose evolution was based on the slip rate. Others, such as Cheong et al. (2007), used a dislocation density approach, which was further detailed into the dislocation components by Patra and McDowell (2012).

Here, an accumulated slip term which accounts for the interaction between slip systems is used to account for both dislocation glide and climb from time-independent plasticity and creep processes. Adopting this approach within a discretised CP framework has two major advantages. First, it captures the local effects of deformation within grains of known crystallographic orientation. Second, the influence of incompatibilities between neighbouring grains which contribute to short-range stresses, are implicitly captured.

6.2. Creep enabled CP model

The hardening approach proposed in this paper, which uses a softening term ($\mathfrak{s}$) in the constitutive equation, models the glide and climb of dislocations and is valid in the primary and secondary creep regimes. At room temperature, $\mathfrak{s} = 1$. However, at higher temperatures $\mathfrak{s}$ progressively reduces from 1 to a saturation value. The value of $\mathfrak{s}$ is determined by the local effective stress found within the polycrystal model. The rate of evolution of $\mathfrak{s}$ is coupled with the change in temperature, with higher temperatures causing $\mathfrak{s}$ to reach steady state sooner, thereby increasing the creep strain rate.

As stresses redistribute within the polycrystal, the hardening term scaled by $\mathfrak{s}$ reduces as $\mathfrak{s}$ evolves, thereby leading to further inelastic strain accumulation. This inelastic strain accumulation is required to maintain the applied load level. Mechanistically this reflects the fact that dislocations glide during primary creep and progressively become pinned at obstacles. By reducing the obstacle strength, further accumulation of inelastic strain is achieved during secondary creep. In order to transition into tertiary creep, other mechanisms such as grain boundary sliding (Stevens, 1972), cavitation (Burnett et al., 2015), and strain localisation effects (Mataya and Carr, 1982) must be considered. These effects could be readily incorporated into the current framework and thus construct a full life creep model.

Furthermore, the von Mises stress found locally is adopted as the dislocation driving force through the softening parameter ($\mathfrak{s}$). The von Mises stress provides a measure of distortion which prevents creep under conditions of high local triaxiality. Other components of stress, such as the maximum local principal stress, will permit creep despite high triaxiality making them inaccurate under certain conditions. Use of the von Mises stress is thus a reasonable driving force to adopt.

6.3. Influence of prior cyclic plasticity on creep

The creep behaviour of the material subjected to prior cyclic plastic loading is investigated numerically and compared with previous experimental results. The cyclic pre-strain has been applied so to reach peak hardening, followed by forward creep at 250 MPa. The effect on accumulated hardening may be explored by considering the results of the simulations. The CP model successfully captures the slower accumulation of creep strain following the application of prior cyclic pre-strain. This is attributed to the development of hardening structures in the CP polycrystal comparable to the dislocation structures developed experimentally. Earlier studies by Mayama et al. (2007) showed a link between hardening and dislocation evolution. They subjected a stainless steel specimen to prior cyclic loading which led to the development of dislocation structures. These structures were more pronounced at higher levels of applied cyclic loading. Upon reaching saturation, however, small changes in the dislocation structures were observed which lead to increased elastic strain during subsequent uniaxial deformation.

The effects of the internal stress state developed during cyclic pre-strain were also simulated successfully. The CP model was subjected to cyclic pre-strain ending in tension and compression, followed by the application of forward creep at 250 MPa. The forward creep stress level required to attain similar levels of creep strain were then estimated and the difference calculated in order to evaluate the influence of the internal stress state on creep. Only small differences in stress levels are observed as seen in Table 1, regardless of the number of cycles applied. A small influence of cyclic pre-straining on creep is reasonable once peak hardening is attained. Prior to attaining this state, however, the internal state developed following final unloading in tension versus compression is expected to be larger. Chen et al. (2015) investigated the role of residual stresses on directionality of hardening in austenitic stainless steel and showed it to be significant prior to peak hardening. This implies that the current model, whilst accurate at capturing peak hardening and its effect on creep, cannot be applied in its current form to investigate intermediate states. Specifically, it is apparent that any internal stress associated with a tension/compression asymmetry on subsequent creep does not result from the incompatibility between grains in the equiaxed random texture which was employed here, hence must manifest in the underlying constitutive relation. Future work are planned to experimentally measure the exact influence of cyclic pre-strain ending in tension and compression. This will aid calibrating the cyclic hardening rule in the current CP framework and account for the directionality of hardening.

6.4. Industrial implication and future application of the current model

The success of the current creep model, coupled with the ability of the crystal plasticity finite element method, in capturing the local effects of deformation has provided an important tool to investigate primary and secondary creep in stainless steel. The ability to predict the subsequent creep evolution under a range of pre-strain regimes provides useful insights into material response during thermal plant operations. Start-up and shutdown of a power plant induces differing states of plasticity into the material. This, coupled with the influence of temperature, influences the stress states developed in the material. Such responses can now be investigated using the CP model presented in this work. A key aspect is the effect of compressive plastic yielding on subsequent tensile creep behaviour.

Furthermore, the current framework may be used to investigate the evolution of elastic residual lattice strains developed in polycrystals during primary and secondary creep. Effects of other mechanical loadings on the creep behaviour of materials can also be investigated. For example, effects of steep stress gradients, non-proportionality of strain and stress, variance of triaxiality factor variation due to notches (Hayhurst et al., 1978), residual stresses (Chen et al., 2014) and elastic follow-up (Smith, 2009). The framework presented provides a methodology which may be validated against previous experimental studies, such as those by Chen et al. (2014), Chen et al. (2015) and Hu et al. (2016).

The current model can also be further improved. For example,

i. The experiments against which the proposed framework was validated and verified were all carried out at a single constant temperature (550 °C). It is therefore necessary to investigate the validity of the framework considering different temperatures. This will provide more justification to the temperature dependent evolution of $\mathfrak{s}$, shown in Fig. 7(b).

ii. Improving the hardening rule to account for directionality under tensile and compressive deformation which is not captured by the underlying microstructure.
iii. It is possible to improve the unifying creep factor to capture tertiary creep mechanisms and damage.
iv. Twin formation is also possible during deformation and can be implemented within the CP framework (Abdolvand et al., 2011).

7. Conclusions

An approach to calculate primary and secondary creep strain was presented within a crystal plasticity finite element framework for 316H stainless steel. Although, it is worth highlighting that the same model can be extended to predict creep behaviour of other materials. A total inelastic strain approach, which does not distinguish between plastic strain and creep strain, was adopted since they both originate from dislocation glide. Plastic strain and creep strain are distinct, however, in that plastic strain is caused by time-independent dislocation glide and creep strain is caused by time-dependent climb assisted dislocation glide. The conventional glide-based plasticity framework was enhanced to account for climb-assisted glide. This was achieved by modifying the slip behaviour of the material using a microstructurally informed dislocation climb softening factor term. The time-independent framework was first calibrated using conventional plasticity data at 823K. Following this, the time-independent properties were fixed and used to calibrate the time-dependent properties using experimental forward creep data for a range of applied stresses. The fully calibrated framework was then used to predict the effect of prior cyclic plasticity on creep.

The results provided the following insights:

i. The rate of creep strain accumulation is slower following prior cyclic plasticity. This is attributed to the development of hardening structures during the cyclic pre-strain phase and is well captured by the model.
ii. The accumulated hardening during cyclic pre-strain is a prerequisite to determining creep strain accumulation under forward creep.
iii. The influence of internal stress (at a grain to grain or intergranular level) on creep is observed to be small which may be a reflection of the use of an equiaxed microstructure with little texture.
iv. Prior to stabilization, the intragranular internal stress state evolution is important due to the influence of kinematic effects which are more prevalent in this phase. The current CP model is unable to capture any differences prior to stabilization. This is attributed to the current lack of directionality in terms of the accumulation of hardening.
v. The capability of the model to predict real forward creep behaviour and the effects of prior cyclic loading at peak hardening makes the model a powerful framework. It will be developed further to include hardening directionality effects which are hypothesized to influence the evolution of the internal stress state and consequently, affect creep evolution.

Acknowledgement

The authors gratefully acknowledge the support of EDF Energy. Dr D Dean. Mr M. Spindler and Dr M Chevalier, EDF Energy, are thanked for their useful discussions.

References

Abdolvand, H., Daymond, M.R., Mareau, C, 2011. Incorporation of twinning into a crystal plasticity finite element model: evolution of lattice strains and texture in Zircaloy-2. Int. J. Plast. 27, 1721–1738.
Agarwal, S., Briant, C.L., Krajewski, P.E., Bower, A.F., Taleff, E.M., 2007. Experimental validation of two-dimensional finite element method for simulating constitutive response of polycrystals during high temperature plastic deformation. J. Mater. Eng. Perform. 16, 170–178.
ASTM International. Designation: E8/E8M – 16a, 2016. Standard Test Methods for Tension Testing of Metallic Materials, 1 doi:10.1520/E0008_E0008M-16A.
Bower, A.F., Wininger, E, 2004. A two-dimensional finite element method for simulating the constitutive response and microstructure of polycrystals during high temperature plastic deformation. J. Mech. Phys. Solids 52, 1289–1317.
Burnett, T.L., Geurts, R., Jazaeri, H., Northover, S.M., McDonald, S.A., Haigh, S.J., Bouchard, P.J., Withers, P.J., 2015. Multiscale analysis of creep cavities and secondary phases in aged AISI type 316 stainless steel. Mater. Sci. Technol. 31, 522–534.
Chen, B, Hu, JN, Wang, YQ, Zhang, S.Y., Petegem, SVan, Cocks, ACF, Smith, D.J., 2015. Role of the misfit stress between grains in the Bauschinger effect for a polycrystalline material. Acta Mater 85, 229–242.
Chen, B., Hu, J.N., Flewitt, P.E.J., Smith, D.J., Cocks, A.C.F., Zhang, S.Y., 2014. Quantifying internal stress and internal resistance associated with thermal ageing and creep in a polycrystalline material. Acta Mater 67, 207–219.
Cheong, K.S., Smillie, M.J., Knowles, D.M., 2007. Predicting fatigue crack initiation through image-based micromechanical modeling. Acta Mater 55, 1757–1768.
Danas, K., Deshpande, V.S., 2013. Plane-strain discrete dislocation plasticity with climb-assisted glide motion of dislocations. Model. Simul. Mater. Sci. Eng. 21.
Dunne, E., Hayhurst, D.R., 1991. An expert system for the determination of creep constitutive equations based on continuum damage mechanics. Journal of Strain Analysis 26 (3).
Dunne, F.P.E., Othman, A.M., Hall, F.R., Hayhurst, D.R., 1990. Representation of uniaxial creep curves using continuum damage mechanics. Int. J. Mech. Sci. 32, 945–957.
Dunne, F.P.E., Rugg, D., Walker, A, 2007. Lengthscale-dependent, elastically anisotropic, physically-based hcp crystal plasticity: application to cold-dwell fatigue in Ti alloys. Int. J. Plast. 23, 1061–1083.
Dyson, B, 2000. Use of CDM in materials modeling and component creep life prediction. J. Press. Vessel Technol. 122, 281.
Edward, G.H., Ashby, M.F., 1979. Intergranular fracture during power-law creep. Acta Metall. 27, 1505–1518.
Erinosho, T.O., Cocks, A.C.F., Dunne, F.P.E., 2013a. Texture, hardening and non-proportionality of strain in BCC polycrystal deformation. Int. J. Plast. 50, 170–192.
Erinosho, T.O., Cocks, A.C.F., Dunne, F.P.E., 2013b. Coupled effects of texture, hardening and non-proportionality of strain on ductility in ferritic steel. Comput. Mater. Sci. 80, 113–122.
Erinosho, T.O., Dunne, F.P.E., 2014. Lattice strain distributions due to elastic distortions and GND development in polycrystals. J. Mech. Phys. Solids 67, 62–86.
Esztergar, E.P., 1972. Creep-fatigue interaction and cumulative damage evaluations for type 304 stainless steel. ORNL 4757.
Forest, S., Rubin, M.B., 2016. A rate-independent crystal plasticity model with a smooth elastic-plastic transition and no slip indeterminacy. Eur. J. Mech. A Solids 55, 278–288.
Geers, M.G.D., Cottura, M., Appolaire, B., Busso, E.P., Forest, S., Villani, A, 2014. Coupled glide-climb diffusion-enhanced crystal plasticity. J. Mech. Phys. Solids 70, 136–153.
Golden, B.J., Li, D.F., O'Dowd, N.P., Tiernan, P., 2014. Microstructural modeling of P91 martensitic steel under uniaxial loading conditions. J. Press. Vessel Technol. 136, 1–6.
Hayhurst, D.R., Leckie, F.A., M, C.J., 1978. Creep rupture of notched bars. Proc. R. Soc. Lond. A 360, 243–264.
Hong, S.M., Min, D.J., Chung, Y.k., Kim, J.H., Kim, D.I., Suh, J.Y., Shim, J.H., Jung, W.S., Choi, I.S., 2016. Effect of preexisting plastic deformation on the creep behavior of TP347 austenitic steel. Mater. Sci. Eng. A 654, 390–399.
Hu, J., Chen, B., Smith, D.J., Flewitt, P.E.J., Cocks, A.C.F., 2016. On the evaluation of the Bauschinger effect in an austenitic stainless steel - The role of multi-scale residual stresses. Int. J. Plast. 84, 203–223. doi:10.1016/j.ijplas.2016.05.009.
Hu, J., Cocks, A.C.F., 2016. A multi-scale self-consistent model describing the lattice deformation in austenitic stainless steels. Int. J. Solids Struct. 78–79, 21–37.
Joseph, T.D., McLennon, D., Spindler, M.W., Truman, C.E., Smith, D.J., 2013. The effect of prior cyclic loading variables on the creep behaviour of ex-service type 316H stainless steel. Mater. High Temp. 30, 156–160.
Keralavarma, ShyamM., Cagin, T., Arsenlis, A., Amine Benzerga, A., 2012. Power-law creep from discrete dislocation dynamics. Phys. Rev. Lett. 109.
Kysar, J., 1997. Addendum to a user-material subroutine incorporating single crystal plasticity in the ABAQUS finite element program. Mech. Rep 1–3.
Lee, E.H., 1969. Elastic–plastic deformation at finite strains. J. Appl. Mech. 36, 1–6.
Li, D.F., Golden, B.J., O'Dowd, N.P., 2014. Multiscale modelling of mechanical response in a martensitic steel: a micromechanical and length-scale-dependent framework for precipitate hardening. Acta Mater 80, 445–456.
Manonukul, A., Dunne, F.P.E., Knowles, D, 2002. Physically-based model for creep in nickel-base superalloy C263 both above and below the gamma solvus. Acta Mater 50, 2917–2931.
Marnier, G., Keller, C., Taleb, L, 2016. Tensile prestrain memory effect on subsequent cyclic behavior of FCC metallic materials presenting different dislocations slip modes. Int. J. Plast. 78, 64–83.
Mataya, M.C., Carr, M.J., 1982. G. K. Flow localization and shear band formation in a precipitation strengthened austenitic stainless steel. Metall. Trans. A 13, 1263–1274.
Mayama, T., Sasaki, K., Narita, Y, 2007. Quantitative evaluation of dislocation structure induced by cyclic plasticity. Key Eng. Mater. 345–346, 49–52.

McGinty, R.D., McDowell, D.L., 2004. Application of multiscale crystal plasticity models to forming limit diagrams. J. Eng. Mater. Technol. 126, 285.
Mehmanparast, A., Davies, C.M., Dean, D.W., Nikbin, K, 2013. Material pre-conditioning effects on the creep behaviour of 316H stainless steel. Int. J. Press. Vessel. Pip. 108–109, 88–93.
Mehmanparast, A., Davies, C.M., Dean, D.W., Nikbin, K, 2016. Effects of plastic pre-straining level on the creep deformation, crack initiation and growth behaviour of 316H stainless steel. Int. J. Press. Vessel. Pip. 141, 1–10.
Mikami, M., 2016. Effects of dislocation substructure on creep deformation. J. Iron. Steel Inst. Jpn. 56 (10), 1840–1846.
Murakami, SS, Kawai, MM, Y, Y., 1990. Creep after cyclic-plasticity under multiaxial conditions for type 316 stainless steel at elevated temperature. ASME J. Eng. Mater. Technol. 112, 346–352.
Patra, A., McDowell, D.L., 2012. Crystal plasticity-based constitutive modelling of irradiated bcc structures. Philos. Mag. 92, 861–887.
Pommier, H., Busso, E.P., Morgeneyer, T.F., Pineau, A, 2016. Intergranular damage during stress relaxation in AISI 316L-type austenitic stainless steels: effect of carbon, nitrogen and phosphorus contents. Acta Mater 103, 893–908.
Roters, F., et al., 2010. Overview of constitutive laws, kinematics, homogenization and multiscale methods in crystal plasticity finite-element modeling: theory, experiments, applications. Acta Mater 58, 1152–1211.
Skelton RP, H.C., 1999. The effect of thermal ageing and mechanical exposure on low cycle creep-fatigue strength of 316 steel at 625 degrees. C. Mater High Temp. 16, 87–97.
Smith, D.J., McFadden, J., Hadidimoud, S., Smith, A.J., Stormonth-Darling, A.J., Abd Aziz, A.A., 2009. Elastic follow-up and relaxation of residual stresses. Proc. IMechE 224, 777–787.
Stevens, R.N., 1972. Grain boundary sliding and diffusion creep. Surf. Sci. 31, 543–565.
Sun, C.Y., Guo, N., Fu, M.W., Wang, S.W., 2016. Modeling of slip, twinning and transformation induced plastic deformation for TWIP steel based on crystal plasticity. Int. J. Plast. 76, 186–212.
Takahashi, 2015. Effect of cyclic loading on subsequent creep behaviour and its implications in creep-fatigue life assessment. Mater. High Temp. 32, 492–501.
Venkatramani, G., Ghosh, S., Mills, M., 2007. A size-dependent crystal plasticity finite-element model for creep and load shedding in polycrystalline titanium alloys. Acta Mater 55, 3971–3986.
Webster, G.A., Ainsworth, R.A., 1994. High Temperature Component Life Assessment. Chapman & Hall.
Weertman, J., 1955. Theory of steady-state creep based on dislocation climb. J. Appl. Phys. 26, 1213–1217.
Wei, K., Dyson, B.F., 1982. Creep-fatigue interactions in 316 stainless steel under torsional loading. In: Conf. Mech. Behav. Nucl. Appl. Stainl. Steel Elev. Temp., 80, pp. 136–144.